J|A|C|S
ARTICLES
Published on Web 07/13/2006

Comparison of Thermodynamic and Kinetic Aspects of Oxidative Addition of PhE−EPh (E = S, Se, Te) to $Mo(CO)_3(PR_3)_2$, $W(CO)_3(PR_3)_2$, and $Mo(N[^tBu]Ar)_3$ Complexes. The Role of Oxidation State and Ancillary Ligands in Metal Complex Induced Chalcogenyl Radical Generation

James E. McDonough, John J. Weir, Kengkaj Sukcharoenphon, Carl D. Hoff,* Olga P. Kryatova, Elena V. Rybak-Akimova,* Brian L. Scott, Gregory J. Kubas,* Arjun Mendiratta, and Christopher C. Cummins*

Contribution from the University of Miami, Coral Gables, Florida 33124, Tufts University, Medford, Massachusetts 02155, Massachusetts Institute of Technology, 77 Massachusetts Avenue, Cambridge, Massachusetts 02139, and Los Alamos National Laboratory, Structural Inorganic Chemistry Group, Chemistry Division, MS J514, Los Alamos National Laboratory, Los Alamos, New Mexico 87545

Received May 9, 2006; E-mail: c.hoff@miami.edu

Abstract: Enthalpies of oxidative addition of PhE−EPh (E = S, Se, Te) to the M(0) complexes $M(P^iPr_3)_2(CO)_3$ (M = Mo, W) to form stable complexes $M(^\bullet EPh)(P^iPr_3)_2(CO)_3$ are reported and compared to analogous data for addition to the Mo(III) complexes $Mo(N[^tBu]Ar)_3$ (Ar = 3,5-$C_6H_3Me_2$) to form diamagnetic Mo(IV) phenyl chalcogenide complexes $Mo(N[^tBu]Ar)_3(EPh)$. Reactions are increasingly exothermic based on metal complex, $Mo(P^iPr_3)_2(CO)_3$ < $W(P^iPr_3)_2(CO)_3$ < $Mo(N[^tBu]Ar)_3$, and in terms of chalcogenide, PhTe−TePh < PhSe−SePh < PhS−SPh. These data are used to calculate L_nM−EPh bond strengths, which are used to estimate the energetics of production of a free $^\bullet$EPh radical when a dichalcogenide interacts with a specific metal complex. To test these data, reactions of $Mo(N[^tBu]Ar)_3$ and $Mo(P^iPr_3)_2(CO)_3$ with PhSe−SePh were studied by stopped-flow kinetics. First- and second-order dependence on metal ion concentration was determined for these two complexes, respectively, in keeping with predictions based on thermochemical data. ESR data are reported for the full set of bound chalcogenyl radical complexes $(PhE^\bullet)M(P^iPr_3)_2(CO)_3$; *g* values increase on going from S to Se, to Te, and from Mo to W. Calculations of electron densities of the SOMO show increasing electron density on the chalcogen atom on going from S to Se to Te. The crystal structure of $W(^\bullet TePh)(P^iPr_3)_2(CO)_3$ is reported.

Introduction

The thiyl radical, whether free[1] ($^\bullet$SR) or bound to a metal complex[2] ($L_nM(^\bullet SR)$), has received increasing attention for its role in biological chemistry.[3] The most common sources of thiyl radicals are (i) oxidation of thiols or thiolates and (ii) radical cleavage of the sulfur−sulfur bond of disulfides. The latter process may be important for transition metal complexes, including metalloenzymes; however it is not clear under what conditions interaction of disulfides with metal complexes will lead to radical generation.

Two mechanisms for reaction of a metal complex with a disulfide are shown in Scheme 1. In the upper reaction manifold, a single metal center reversibly binds a disulfide and then is capable of direct splitting of the sulfur−sulfur bond. This

Scheme 1

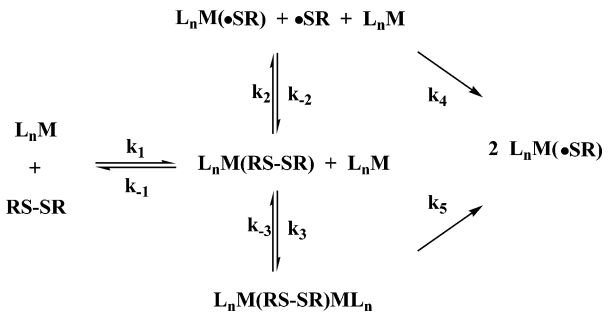

generates a free radical, which in the presence of additional metal complex would be rapidly trapped. However in an enzymatic or catalytic process under conditions of low intercepting metal complex concentration, a thiyl radical so generated could conceivably take part in secondary reactions. The upper pathway can have a low enthalpy of activation only if the M−SR bond is stronger than the RS−SR bond. The lower pathway would be expected to be operative for complexes with weak

(1) Wardman, P. In *Sulfur Centered Radicals*; Alfassi, Z. B., Ed.; John Wiley: New York, 1999.
(2) Kimura, S.; Bill, E.; Bothe, E.; Weyhermuller, T.; Wieghardt, K. *J. Am. Chem. Soc.* **2001**, *123*, 6025.
(3) (a) Bennati, M.; Robblee, J. H.; Mugnaini, V.; Stubbe, J.; Freed, J. H.; Borbat, P. *J. Am. Chem. Soc.* **2005**, *127*, 15014. (b) Stubbe, J.; Nocera, D. G.; Yee, C. S.; Chang, C. Y. *Chem. Rev.* **2003**, *103*, 2167. (c) Licht, S. S.; Booker, S.; Stubbe, J. *Biochemistry* **1999**, *38*, 1221.

10.1021/ja063250+ CCC: $33.50

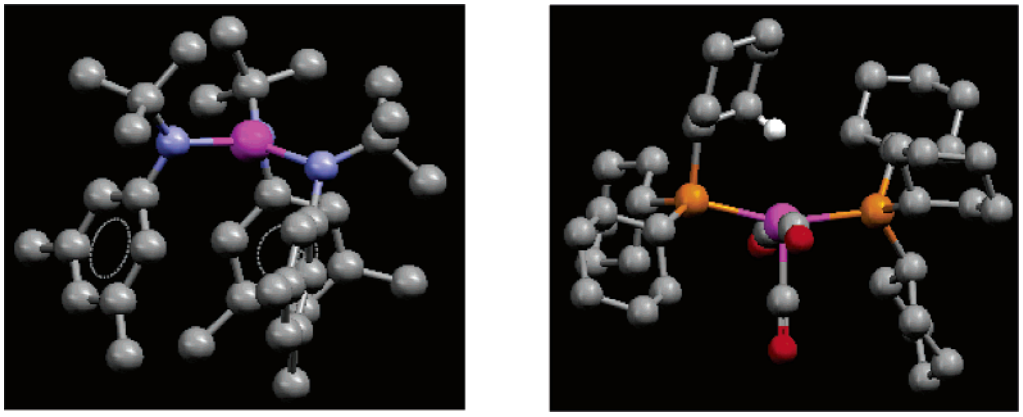

Figure 1. Ball-and-stick representations of $Mo(N[^tBu]Ar)_3$ and $Mo(PCy_3)_2(CO)_3$ highlighting the vacant sites available for approach to an incoming ligand.

individual M−SR bonds. Derived rate laws for these reactions are complex[4] and depend on the relative magnitudes of the specific rate constants, so that in practice it can be difficult to distinguish between them on kinetic data alone.

Despite the importance of oxidative addition of disulfides at metal centers, relatively few detailed mechanistic studies have been reported. Earlier work[5] has shown that for the 17-electron radical complex $^{\bullet}Cr(CO)_3Cp^*$ reaction with PhS−SPh is first-order in metal radical and generates free $^{\bullet}SPh$, but that due to its stronger sulfur−sulfur bond, reaction with MeS−SMe obeys a rate law second-order in metal complex. In the case of the 16-electron fragments M(phen)$(CO)_3$ (M = Mo, W) concerted attack by two metal centers was found to occur.[6] Bergman and Aubart[7] investigated reaction of a range of aryl disulfides with both $CoCp_2$ and $Cp_2Ta(\mu\text{-}CH_2)_2CoCp$. Strong dependence on the electrostatic character of the specific disulfide for $CoCp_2$ showed that oxidative addition proceeded mainly by outer-sphere electron transfer, but that $Cp_2Ta(\mu\text{-}CH_2)_2CoCp$ reacted with substantially more covalent character in the transition state.

This paper reports detailed investigation of reactivity of the phenyl dichalcogenides (PhE−EPh, E = S, Se, Te) with three metal complexes $M(CO)_3(PR_3)_2$ (M = Mo, W) and $Mo(N[R]Ar)_3$. Despite different oxidation states and ancillary ligands, both of these complexes present a vacant site at the metal for ligand binding and oxidative addition, as shown in Figure 1.

The complexes $M(CO)_3(PR_3)_2$ (M = Cr, Mo, W; R = ^{i}Pr, Cy)[8] are formally 16-electron complexes with no unpaired electrons. However, saturation at the metal and achievement of an 18 valence electron count is attained to some extent since the vacant site is blocked by a three-center M···H−C agostic bond. Despite the steric crowding at the metal center in $M(CO)_3(PR_3)_2(L)$, ligand substitution reactions are facile. Kinetic evidence indicates they are even associative in character, i.e., a concerted process where the agostic C−H "pushes off" as the incoming group in turn displaces the agostic interaction.[8b] Binding of H_2 yields a molecular hydrogen complex that exists in tautomeric equilibrium with a dihydride. Dinitrogen binds reversibly to form mononuclear $M(CO)_3(PCy_3)_2(N_2)$, and in the case of the sterically less crowded isopropyl phosphine a dinuclear complex $[\mu\text{-}N_2][W(CO)_3(P^iPr_3)_2]_2$ is formed as well. The crystal structure of this complex has been determined;[8c] however splitting of dinitrogen does not occur for these low-valent complexes.

In contrast the complex[9] $Mo(N[R]Ar)_3$ has three unpaired electrons in its ground state and shows little tendency to bind conventional ligands for both steric and electronic reasons. For the sterically less crowded R = isopropyl derivative, an agostic interaction is not present, but rather the potential three-center agostic C−H bond undergoes oxidative addition to form a molybdaziridine hydride complex of Mo(V). The latter has been shown in many cases to act as a "resting state" for the active $Mo(N[R]Ar)_3$. Binding of dinitrogen to yield a detectable mononuclear adduct $[N_2][Mo(N[R]Ar)_3]$ does not occur under normal conditions, but at low temperature a dinuclear intermediate $[\mu\text{-}N_2][Mo(N[R]Ar)_3]_2$ is formed and subsequently splits dinitrogen to form 2 mol of the terminal nitrido complex $N{\equiv}Mo(N[R]Ar)_3$.

Despite chemical differences described above, the phosphine and amido complexes shown in Figure 1 each present an open site for ligand binding as well as oxidative addition reactions. In addition they provide an opportunity to compare and contrast

(4) The derived rate law for the upper manifold is $dP/dt = 2k_1k_2k_4[ML_n]^2[RSSR]/\{k_{-1}k_{-2}[ML_nSR] + k_4[ML_n]\}$. The derived rate law for the lower manifold is $dP/dt = 2k_1k_3[ML_n]^2[RSSR]/\{k_{-1}k_{-3} + k_{-1}k_5 + k_3k_5[ML_n]\}$. Due to the complexity of these equations, depending on the exact values of the specific rate constants, as well as reagent concentrations, a range of behavior could in principle be displayed. However, under most circumstances the upper manifold would be expected to reduce to first-order dependence on metal complex concentration, and the lower manifold to second-order dependence on metal complex concentration. In the case that $[ML_nSR] = 0$ the upper pathway reduces to $dP/dt = 2k_1k_2[ML_n][RSSR] = k_{obs}[ML_n][RSSR]$ where $k_{obs} = 2k_1k_2$. For the lower pathway for low relative values of $[ML_n]$ the rate law reduces to $dP/dt = 2k_1k_3[ML_n]^2[RSSR]/k_{-1}\{k_{-3} + k_5\} = k_{obs}[ML_n]^2[RSSR]$ where $k_{obs} = 2k_1k_3/k_{-1}\{k_{-3} + k_5\}$. Due to the rapid nature of the reaction, values of k_{obs} are measured in this work and frequently could not be resolved into the individual rate constants shown in this representative scheme.

(5) Ju, T. D.; Capps, K. B.; Lang, R. L.; Roper, G. C.; Hoff, C. D. *Inorg. Chem.* **1997**, *36*, 614.
(6) Ju, T. D.; Capps, K. B.; Roper, G. C.; Hoff, C. D. *Inorg. Chim. Acta* **1998**, *270*, 488.
(7) Aubart, M.; Bergman, R. G. *J. Am. Chem. Soc.* **1998**, *120*, 8755.
(8) (a) Wasserman, H. J.; Kubas, G. J.; Ryan, R. H. *J. Am. Chem. Soc.* **1986**, *108*, 2294. (b) Zhang, K.; Gonzalez, A. A.; Mukerjee, S. L.; Chou, S.-J.; Hoff, C. D.; Kubat-Martin, K. A.; Barnhart, D.; Kubas, G. J. *J. Am. Chem. Soc.* **1991**, *113*, 9170. (c) Butts, M. D.; Kubas, G. J.; Luo, X.-L.; Bryan, J. C. *Inorg. Chem.* **1997**, *36*, 3341. (d) Gonzalez, A. A.; Zhang, K.; Nolan, S. P.; de la Vega, R. L.; Mukerjee, S. L.; Hoff, C. D.; Kubas, G. J. *Organometallics* **1988**, *7*, 2429. (e) Gonzalez, A. A.; Hoff, C. D. *Inorg. Chem.* **1989**, *28*, 4295. (f) Zhang, K.; Gonzalez, A. A.; Hoff, C. D. *J. Am. Chem. Soc.* **1989**, *111*, 3627. (g) Gonzalez, A. A.; Zhang, K.; Mukerjee, S. L.; Hoff, C. D.; Khalsa, G. R. K.; Kubas, G. *J. ACS Symp. Ser.* **1990**, *428*, 133. (h) Kubas, G. J.; Nelson, J. E.; Bryan, J. C.; Eckert, J.; Wisniewski, L.; Zilm, K. *Inorg. Chem.* **1994**, *33*, 2954.
(9) (a) Laplaza, C. E.; Cummins, C. C. *Science* **1995**, *268*, 861. (b) Laplaza, C. E.; Johnson, A. R.; Cummins, C. C. *J. Am. Chem. Soc.* **1996**, *118*, 709. (c) Laplaza, C. E.; Johnson, M. J. A.; Peters, J.; Odom, A. L.; Kim, E.; Cummins, C. C.; George, G. N.; Pickering, I. J. *J. Am. Chem. Soc.* **1996**, *118*, 8623. (d) Cummins, C. C. *Prog. Inorg. Chem.* **1998**, *47*, 685. (e) Tsai, Y.; Johnson, M. J. A.; Mindiola, D. J.; Cummins, C. C.; Klooster, W. T.; Koetzle, T. F. *J. Am. Chem. Soc.* **1999**, *121*, 10426. Tsai, Y.; Cummins, C. C. *Inorg. Chim. Acta* **2003**, *345*, 63.

reactivity involving low and intermediate oxidation states at group 6 metal centers and to probe how oxidation state and ancillary ligand environments influence the ability of a metal complex to generate free chalcogenyl radicals in a single step or bound radicals in a concerted process.

Experimental Section

General Considerations. Unless stated otherwise, all operations were performed in a Vacuum Atmospheres or MBraun drybox under an atmosphere of purified nitrogen or argon or utilizing standard Schlenk tube techniques under argon. Toluene and heptane were purified by distillation under argon from sodium benzophenone ketyl into flame-dried glassware. Methylene chloride was refluxed under an argon atmosphere over P_2O_5 and then distilled. FTIR data were obtained on a Perkin-Elmer system 2000 spectrometer; ESR data, on a Bruker EMX spectrometer utilizing X-band radiation in quartz tubes sealed under vacuum. Stopped-flow kinetic and solution calorimetric data were obtained using techniques analogous to those described previously[8,9,21] and are illustrated with representative procedures below. Dichalcogenides were obtained from Aldrich Chemical and were recrystallized from methylene chloride/heptane mixtures by slow evaporation and cooling.

Preparation of M(•EPh)(CO)$_3$(P^{i}Pr$_3$)$_2$ and Crystal Growth of W(•TePh)(CO)$_3$(P^{i}Pr$_3$)$_2$. Reactions of PhSe−SePh and PhTe−TePh with M(CO)$_3$(P^{i}Pr$_3$)$_2$ were performed in a manner strictly analogous to that reported previously[11] for reaction of PhS−SPh. The reactions were rapid and quantitative, as determined by FTIR spectroscopy. In the glovebox a solution of (μ^2-N$_2$)[W(CO)$_3$(P^{i}Pr$_3$)$_2$]$_2$ (0.15 g) was prepared in a Schlenk tube under Ar in 15 mL of freshly distilled toluene. Three milliliters of this yellow-orange solution containing 2.5×10^{-2} mmol of the dinuclear complex was added by syringe to 5.4 mg (2.50×10^{-2}) mmol of PhS−SPh. The solution immediately turned a deep blue color, and gas was evolved. Analysis by FTIR spectroscopy showed quantitative conversion to product as shown in Supporting Information Figure S1. Similar equimolar reaction of 3.0 mL of this solution with PhSe−SePh (7.7 mg) or PhTe−TePh (10.0 mg) resulted in similar rapid and quantitative formation to give blue-green and green complexes, respectively. Solutions of these complexes overnight in the glovebox showed little sign of decomposition for W derivatives, but were less stable for the Mo derivatives. ESR spectroscopy was done by sealing toluene solutions in quartz tubes under vacuum. These tubes left in the freezer were found to be stable for a period of weeks to months for the W derivatives, but showed some slow decomposition for the Mo complexes.

Crystals of W(•TePh)(CO)$_3$(P^{i}Pr$_3$)$_2$ suitable for structure determination were prepared by reaction of 0.1 g of W(CO)$_3$(P^{i}Pr$_3$)$_2$ and 0.035 g of PhTeTePh in 10 mL of toluene. Upon addition of toluene, the solution turned the deep blue color characteristic of the radical W(•TePh)(CO)$_3$(P^{i}Pr$_3$)$_2$. Approximately 2 mL of this solution was filtered into a glass tube under argon, then layered with 8 mL of distilled heptane. The tube was sealed and placed in a freezer for a period of 2 weeks. During that time slow diffusion of the two solvents occurred and blue-purple crystals formed. The tube was opened in the glovebox, and the mother liquor was removed by syringe and replaced with a small amount of degassed mineral oil. The tube was then sealed again and stored until mounting for structure determination.

Crystal Structure Determination. Due to air sensitivity, a crystal of W(•TePh)(CO)$_3$(P^{i}Pr$_3$)$_2$ was mounted from a pool of mineral oil under argon gas flow. The crystal was placed on a Bruker P4/CCD diffractometer and cooled to 203 K using a Bruker LT-2 temperature device. The instrument was equipped with a sealed, graphite-monochromatized Mo Kα X-ray source ($\lambda = 0.71073$ Å). A hemisphere of data was collected using φ scans, with 30 s frame exposures and 0.3° frame widths. Data collection and initial indexing and cell refinement were handled using SMART[10a] software. Frame integration, including Lorentz−polarization corrections, and final cell parameter calculations were carried out using SAINT software.[10b] The data were corrected for absorption using the SADABS program.[10c] Decay of reflection intensity was monitored via analysis of redundant frames. The structure was solved using direct methods and difference Fourier techniques, and two crystallographically independent molecules were identified in the unit cell. All hydrogen atom positions were idealized and rode on the atom they were attached to. After all atomic positions were assigned and refined anisotropically to conversion, four significant residual peaks (two at 15 e Å^{-3} and two at 8 e Å^{-3}) remained in the difference map. These four peaks were refined as two sets of W−Te twin components based on their distances and locations. The site occupancy factors were tied to the major W−Te components and refined to approximately a 13% contribution; to obtain convergence, the major and minor contributions were fixed at 0.87 and 0.13, respectively. The final refinement included anisotropic temperature factors on all non-hydrogen atoms, except for the minor Te and W component atoms. Structure solution, refinement, graphics, and creation of publication materials were performed using SHELXTL.[10d] Additional details of data collection and structure refinement are listed in Table 1. The refinement of the W(•TePh)(CO)$_3$[P^{i}Pr$_3$]$_2$ molecule in a major 87% occupied site and a minor 13% occupied site is an example of "whole molecule disorder".[10e]

Reaction of M(CO)$_3$(P^{i}Pr$_3$)$_2$ and PhS−SPh and PhSe−SePh under H$_2$ Atmosphere. In a typical procedure a solution of 0.12 g of Mo(CO)$_3$(P^{i}Pr$_3$)$_2$ dissolved in 5 mL of freshly distilled toluene was prepared in a 25 mL Schlenk tube under H_2 (99.9995%) at 1.3 atm of pressure and a temperature of 10 °C. A 1 mL aliquot was removed for FTIR and showed the presence of Mo(CO)$_3$(P^{i}Pr$_3$)$_2$(H$_2$). A solution of 0.05 g of PhS−SPh in 2.5 mL of toluene was then added. The solution turned deep blue, and an FTIR of the solution showed the near

(10) (a) *SMART-NT 4*; Bruker AXS, Inc.: Madison, WI, 1996. (b) *SAINT-NT 5.050*; Bruker AXS, Inc.: Madison, WI, 1998. (c) Sheldrick, G. *SADABS*, first release; University of Göttingen: Germany. (d) *SHELXTL NT* Version 5.10; Bruker AXS, Inc.: Madison, WI, 1997. (e) This phenomenon and the subsequent refinement of the minor contribution are accepted among crystallographers; see for example: Thomas, C. A.; Zong, K. W.; Abboud, K. A.; Steel, P. J.; Reynolds, J. R. *J. Am. Chem. Soc.* **2004,** *126*, 16440. Bradley, C. A.; Keresztes, I.; Lobkovsky, E.; Young, V. G.; Chirik, P. J. *J. Am. Chem. Soc.* **2004**, *126*, 16937. John, K. D.; Miskowski, V. M.; Vance, M. A.; Dallinger, R. F.; Wang, L. C.; Geib, S. J.; Hopkins, M. D. *Inorg. Chem.* **1998**, *37*, 6858.

(11) (a) Lang, R. F.; Ju, T. D.; Kiss, G.; Hoff, C. D.; Bryan, J. C.; Kubas, G. J. *J. Am. Chem. Soc.* **1994**, *116*, 7917. (b) Lang. R. F.; Ju, T. D.; Kiss, G.; Hoff, C. D.; Bryan, J. C.; Kubas, G. J. *Inorg. Chim. Acta* **1997**, *259*, 317. (c) Data were reported in ref 11a for the enthalpy of reaction W(CO)$_3$(P^{i}Pr$_3$)$_2$ + $^1/_2$PhS−SPh with $\Delta H = -18.9 \pm 1.2$ kcal/mol; this compares to data in Table 4 (divided by 2) of $\Delta H = -21.1 \pm 0.5$ kcal/mol. The disagreement between these two values is outside experimental error by 0.5 kcal/mol. The derived data rely on the purity of the PhS−SPh. A possible reason for this slight disagreement is that the current sample was more pure. Care was taken to ensure that the recrystallized dichalogenides were not only spectroscopically pure as judged by NMR data but also of high crystal quality. To compare the three complexes shown in Table 4, samples from the same batches of dichalcogenides were used for each metal.

(12) Remenyi, C.; Kaupp, M. *J. Am. Chem. Soc.* **2005**, *127*, 11399.

(13) Armstrong, D. A.; Chipman, D. M. In *S-Centered Radicals*; Alfassi, ZX. B., Ed.; John Wiley: New York, 1999.

(14) Landolt-Bernstein. *Numerical Data and Functional Relationships in Science and Technolgy*, New Series, Volume 17, *Magnetic Properties of Free Radicals*; Fischer, H., Ed.; Springer-Verlag: Berlin, 1988. See also Vol. 9, Hellwege, K. H. 1979, in this series.

(15) Tripathi, G. N. R.; Sun, Q.; Armstrong, D. A.; Chipman, D. M.; Schuler, R. H. *J. Phys. Chem.* **1992**, *96*, 5344.

(16) The isotropic shift for the SPh radical is reported as 2.008 and SePh as 2.007 in ref 14. The isotropic shift of $SCH_2C_6H_5$ is reported as 2.024 and $SeCH_2C_6H_5$ as 2.102. The authors could not find corresponding data for Te radicals.

(17) Springs, J.; Janzen, C. P.; Darensbourg, M. Y.; Calabrese, J. C.; Krusic, P. J.; Verpeaux, J. N. Amatore, C. *J. Am. Chem. Soc.* **1990**, *112*, 5789−5797.

(18) Rieger, P. H. *Coord. Chem. Rev.* **1994**, *135/136*, 203; see Table 16, p 249.

(19) Witner, A.; Huttner, G.; Zsolnai, L.; Kronick, P.; Gottlieb, M.; Angew. Chem., *Intl. Ed. Engl.* **1984**, *23*, 975. See also: Lau, P.; Braunwarth, H.; Huttner, G.; Gunauer, D.; Evertz, K.; Imhof, W.; Emmerich, C.; Zsolnai, L.; *Organometallics* **1991**, *10*, 3861.

(20) Angerhofer, A. A.; Walker, L.; Sukcahroenphon, K.; McDonough, J. E.; Hoff, C. D. Work in progress.

(21) McDonough, J. E.; Carlson, M. J.; Weir, J. J.; Hoff, C. D.; Kryatova, O. P.; Rybak-Akimova, E. V.; Cummins, C. C. *Inorg. Chem.* **2005**, *44*, 3127.

Table 1. Crystal Structure Parameters for W(•TePh)(CO)$_3$(P^{i}Pr$_3$)$_2$

crystal system	monoclinic
space group (No.)	$P\bar{1}$ (#2)
description	black multifaceted block
cryst size	0.16 × 0.20 × 0.32 mm^3
a, Å	12.154(5)
b, Å	16.218(7)
c, Å	16.684(7)
α, deg	75.872(6)
β, deg	79.373(8)
γ, deg	89.993(8)
volume, Å^3	3131(2)
Z	4
D_{calcd}, g cm^{-3}	1.682
T, K	203

quantitative conversion to Mo(•SPh)(CO)$_3$(P^{i}Pr$_3$)$_2$. The H−SPh band, which is weak and occurs near 2570 cm^{-1} in toluene, could not be quantified above baseline noise, and no odor characteristic of thiophenol was detected. In comparable experiments with W(CO)$_3$(P^{i}Pr$_3$)$_2$, thiophenol was detected both by its characteristic smell and also by the ν(H−SPh) present in the FTIR spectrum. The FTIR intensity data indicated that ∼1/3 mole of HSPh was produced for each mole of reacting W(CO)$_3$(P^{i}Pr$_3$)$_2$ under these conditions. In addition to bands characteristic of W(•SPh)(CO)$_3$(P^{i}Pr$_3$)$_2$ production, extra bands attributed to uncharacterized products were detected. Reactions using PhSe−SePh were performed in a strictly analogous manner. The H−SePh stretch occurs at 2310 cm^{-1} as determined in our experiments, and no instability or decomposition of PhSeH was observed in the absence of air. Under a hydrogen atmosphere, neither Mo(CO)$_3$(P^{i}Pr$_3$)$_2$ nor W(CO)$_3$(P^{i}Pr$_3$)$_2$ was found to produce H−SePh as detected either by odor or by FTIR.

Reaction of Mo(•SePh)(CO)$_3$(P^{i}Pr$_3$)$_2$ and Mo(N[^{t}Bu]Ar)$_3$. In the glovebox a purple solution of 0.255 g of Mo(CO)$_3$(P^{i}Pr$_3$)$_2$ in 5 mL of freshly distilled toluene was prepared in a Schlenk tube. After removing 1 mL of this solution for FTIR, solid PhSe−SePh (0.0580 g) was added to prepare in situ a bright blue solution of Mo(•SePh)(CO)$_3$(P^{i}Pr$_3$)$_2$. To this solution was added 0.19 g of Mo(N[^{t}Bu]Ar)$_3$, and a series of FTIR spectra were run over a period of 2 h. During this time the FTIR spectral bands attributed to Mo(•SePh)(CO)$_3$(P^{i}Pr$_3$)$_2$ at 1981 and 1877 cm^{-1} slowly decreased and bands attributed to Mo(CO)$_3$(P^{i}Pr$_3$)$_2$ at 1955, 1844, and 1813 cm^{-1} grew in.

Stopped-Flow Kinetic Measurements. Toluene solutions of the reagents were prepared in a Vacuum Atmospheres or a MBraun glovebox filled with argon and placed in Hamilton gastight syringes. Time-resolved spectra or single-wavelength kinetic traces were acquired at temperatures from −80 to +25 °C using a Hi-Tech Scientific (Salisbury, Wiltshire, UK) SF-43 multimixing CryoStopped-Flow instrument in a diode array mode or a single-wavelength mode, respectively. The stopped-flow instrument was equipped with stainless steel plumbing, a 1.00 cm stainless steel mixing cell with sapphire windows, and an anaerobic gas-flushing kit. The instrument was connected to an IBM computer with IS-2 Rapid Kinetic software (Hi-Tech Scientific). The temperature in the mixing cell was maintained to ±0.1 K, and the mixing time was 2 to 3 ms. The driving syringe compartment and the cooling bath filled with heptane (Fisher) were flushed with argon before and during the experiments, using anaerobic kit flush lines. All flow lines of the SF-43 instrument were extensively washed with degassed, anhydrous toluene before charging the driving syringes with reactant solutions.

These techniques are illustrated for study of the kinetics of reaction of Mo(N[^{t}Bu]Ar)$_3$ and PhSe−SePh. The reaction was studied by rapid scanning spectrophotometry from −40 to +25 °C under second-order (0.3 mM solutions) and under pseudo-first-order conditions (0.45 mM for Mo complex and 4.5 mM for Ph_2Se_2). The rate dependence on [Ph_2Se_2] was studied at −40 °C using [Ph_2Se_2] = 0.45 mM before mixing and varying [Ph_2Se_2] from a 1- to 20-fold excess, and the reaction order in Ph_2Se_2 was established by method of initial rates. The order in Mo complex was established by changing [Mo complex] (0.45, 0.3375, and 0.225 mM) under pseudo-first-order conditions (4.5 mM Ph_2Se_2). The system was tested using conventional UV−vis spectrometry at room temperature (Figure S2). Regardless of the amount of Ph_2Se_2 added, the characteristic spectra of green Mo(N[^{t}Bu]Ar)$_3$(SePh) were observed. This product is moderately air-stable, showing little decomposition 10 min after the cell was opened to air. The same spectral changes were observed in a stopped-flow cell under any conditions of concentration/temperature. All of the experiments were performed in a single-mixing mode of the instrument, with a 1:1 (v/v) mixing ratio. The reactions were monitored for three to five half-lives. A series of four to six measurements at each temperature gave an acceptable standard deviation (within 10%). Data analysis was performed with IS-2 Rapid Kinetic software from Hi-Tech Scientific, Spectfit/32 Global Analysis System software from Spectrum Software Associates, or Excel Solver from Microsoft.

Calorimetric Measurements. In the glovebox a solution of 0.45 g of W(CO)$_3$(P^{i}Pr$_3$)$_2$ was prepared under argon atmosphere in 6 mL of toluene. One milliliter of this solution was used for recording an FTIR spectrum, and the remaining 5 mL was loaded under argon into the cell of the Setaram-C-80 Calvet microcalorimeter. The solid-containing compartment of the calorimeter was loaded with 0.0103 g of PhS−SPh, which had been recently recrystallized from methylene chloride/heptane and then dried in vacuo. The assembled calorimeter cell was taken from the glovebox and loaded into the calorimeter. Following temperature equilibration the reaction was initiated and the thermogram indicated a rapid reaction, which returned cleanly to baseline with no thermal signal indicative of secondary reactions occurring. Following return to baseline, the cell was taken back into the glovebox and a sample analyzed by FTIR spectroscopy showed the presence of only starting material, product, and trace W(CO)$_4$(P^{i}Pr$_3$)$_2$, which is present whenever handling W(CO)$_3$(P^{i}Pr$_3$)$_2$. The integrated enthalpy of reaction, −37.06 kcal/mol PhS−SPh, was averaged with four other independent measurements to give an average value based on solid PhS−SPh of −36.2 ± 0.6 kcal/mol. Correction for the endothermic enthalpy of solution of solid PhSSPh (+6.0 ± 0.1 kcal/mol) yields the final value with all species in toluene solution of −42.2 ± 0.7 kcal/mol.

Results and Discussion

Preparative and Structural Chemistry. Reaction 1 was found to occur rapidly for E = Se, Te and M = Mo, W:

$$2\ M(CO)_3(PR_3)_2 + PhE{-}EPh \rightarrow 2\ M(^{\bullet}EPh)(CO)_3(PR_3)_2 \quad (1)$$

This is an extension to the heavier chalcogenides of the previously studied[11] oxidative addition of disulfides to the same complexes. From a preparative point of view the initial radical-forming reactions are rapid and quantitative, as determined by FTIR studies. Spectroscopic data for the complexes are summarized in Supporting Information Figure 1.

Previously we had reported the X-ray structure of the 17-electron radical complex W(•I)(CO)$_3$(P^{i}Pr$_3$)$_2$, but all previous attempts to obtain X-ray-quality crystals of the thiolate complex radicals W(•SR)(CO)$_3$(P^{i}Pr$_3$)$_2$ failed.[11] In the present study, slow crystallization from toluene/heptane produced crystals of W(•TePh)(CO)$_3$(P^{i}Pr$_3$)$_2$, the structure of which is shown in Figure 2 and summarized in Table 1.

To the authors' knowledge, the structure in Figure 2 is the first reported for a W(I) chalcogenyl radical complex. The structure is essentially distorted octahedral and resembles that previously reported[11]for W(•I)(CO)$_3$(P^{i}Pr$_3$)$_2$. The W−Te−C(22) angle of 108.23° does not appear to show unusual distortion. It is worth noting that the P−W−P angle of 166.82° is bent down

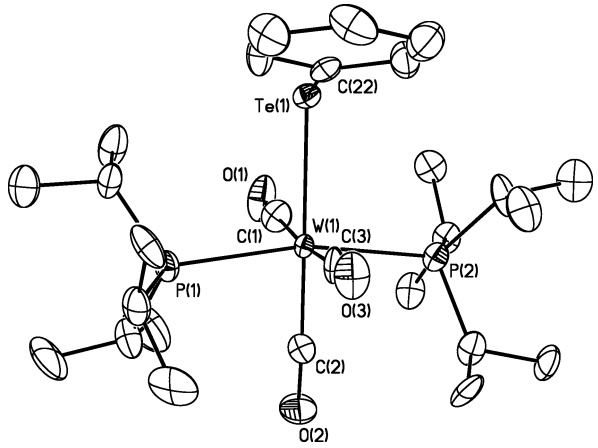

Figure 2. Thermal ellipsoid plot of W(•TePh)$(CO)_3(P^iPr_3)_2$. Selected bond distances (Å) and angles (deg): W(1)−Te(1) = 2.7535(12), W(1)−P(1) = 2.5524(15), W(1)−P(2) = 2.5600(14), W(1)−C(1) = 1.994(5), W(1)−C(2) = 1.956(5), W(1)−C(3) = 2.019(4), C(2)−W(1)−Te(1) = 177.90(14), P(1)−W(1)−P(2) = 166.87(4), C(1)−W(1)−C(3) = 172.31(18). Relevant structural parameters are collected in Table 1; full crystal data are available as Supporting Information.

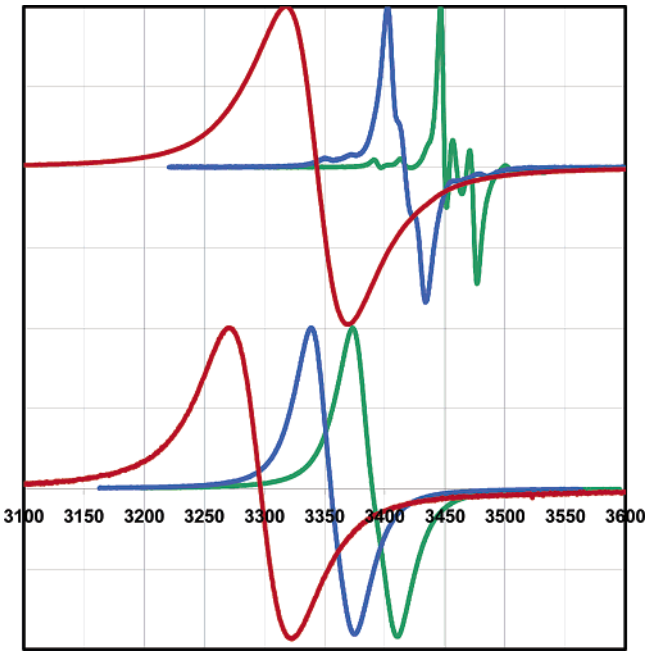

Figure 3. Normalized plots of ESR spectra (room temperature, toluene solution) for M(•EPh)$(CO)_3(P^iPr_3)_2$ radicals: Mo (upper spectra) and W (lower spectra) for S (green), Se (blue), and Te (red). Spectra for TeNaphth (Naphth = naphthyl, not shown for clarity) are virtually identical to those of TePh in terms of position and shape.

away from the W−TePh bond. The Te−W−C(2) bond angle of 177.59° is close to linear.

ESR Studies of M(•EPh)$(CO)_3(P^iPr_3)_2$. The stable free radical complexes prepared here were all characterized by solution phase room-temperature ESR spectroscopy. Recent work[12] has pointed out the difficulty and importance of knowing the location of the unpaired electron in such radical complexes. Two limiting views are (i) a metal-based radical and (ii) a complexed thiyl or chalcogenyl radical. In addition, the organic group can potentially serve as a site of delocalization. The room-temperature ESR spectra of these radical complexes are shown in Figure 3, and measured isotropic *g* values are summarized in Table 2.

Table 2. Isotropic *g* Values for Complexes at Room Temperature in Toluene Solution.

metal	S	Se	Te	Te–Naphth
Mo	2.0372	2.0626	2.1076	2.1075
W	2.0787	2.1003	2.1378	2.1389

Thiyl radicals are known to have broad, poorly resolved ESR spectra[13] with *g* values ranging from 2.0 to 2.25. Data[14] indicate that for •SPh the *g* value is near 2.008, and for •SePh near 2.007. This could be interpreted as indicating some delocalization of the electron into the arene ring for the $•EC_6H_5$ radicals since the *g* value is close to the typical value near 2.003 commonly observed for organic radicals. Theoretical calculations[15] indicate that for •SPh the SOMO is a predominantly sulfur-based S pπ orbital involved to only a minor extent with arene orbitals. The isotropic *g* values for $•SCH_2Ph$ (2.024) and $•SeCH_2Ph$ (2.102) are higher and may reflect even higher localization on the chalcogen. Data for •TePh radicals[16] could not be found by the authors.

A complete set of transition metal M−E−Ph radicals comparable to these for comparison could also not be found by the authors. The metastable radicals $(•SR)(Cr(CO)_5)_2$ formed on low-temperature oxidation of anionic $[RS][Cr(CO)_5]_2^-$ have been studied,[17] and ESR data for these radicals were found to be consistent with formulation as organometallic analogues of sulfuranyl radicals $R_3S•$. Isotropic *g* values were near 2.025 for a range of complexes, and the unpaired electron was believed to be in a predominantly $3p_z$ orbital of the trigonal sulfur. Data for several Mn(II) piano stool complexes $CpMn(CO)_2(X)$ have been collected.[18] Of relevance to this work, Huttner and co-workers[19] have reported isotropic *g* values of 2.03 for Cp*-$(CO)_2Mn(•S^tBu)$ and 2.07 for $Cp^*(CO)_2Mn(•SePh)$. As discussed in the following section, calculations indicate that the SOMO is predominantly a mixture of chalcogen and metal-based orbitals. The nearly identical nature of the ESR data for phenyl and naphthyl derivatives would support little influence of the aromatic ring. Data in Table 2 show increasing *g* values on going from S to Se to Te. That would be in keeping with data discussed above for the $E-CH_2C_6H_5$ derivatives. In addition it should be noted that there is an increase in *g* value on going from Mo to W for all three chalcogens. This could be due to changes in the SOMO or the metal contribution to the *g* value; however more detailed analysis of this point is beyond the scope of this paper. Work in progress on low-temperature ESR and ENDOR on these complexes may yield additional insight.[20]

Calculation of the SOMO for M(•EPh)$(CO)_3(PH_3)_2$ for M = Mo, W; E = S, Te. To address theoretically the question of the odd-electron orbital in complexes of formula M(•EPh)$(CO)_3$-$(PR_3)_2$ (E = S, Se, Te; M = Mo, W), the structure of the representative model system Mo(•SPh)$(CO)_3(PH_3)_2$ was optimized. The multipole-derived spin density (MDC-q) on the atoms was inspected and its SOMO visualized. From the output of the Amsterdam Density Functional (ADF) calculation, only a few atoms had significant spin density (Table 3). These results indicate that the unpaired electron is located primarily on the Mo and S atoms with some spin density on the carbonyl trans to the SPh ligand. The values above are quite consistent with the appearance of the SOMO, shown in Figure 4. The role of the chalcogenide was investigated by doing a similar geometry optimization and analysis for E = Te. The complex Mo(•TePh)-

Table 3. Calculated Spin Densities for Mo(•SPh)$(CO)_3(PH_3)_2$

	MDC-q spin density
Mo	−0.361
S	−0.356
C	−0.110
O	−0.070
P	−0.038
P	−0.012

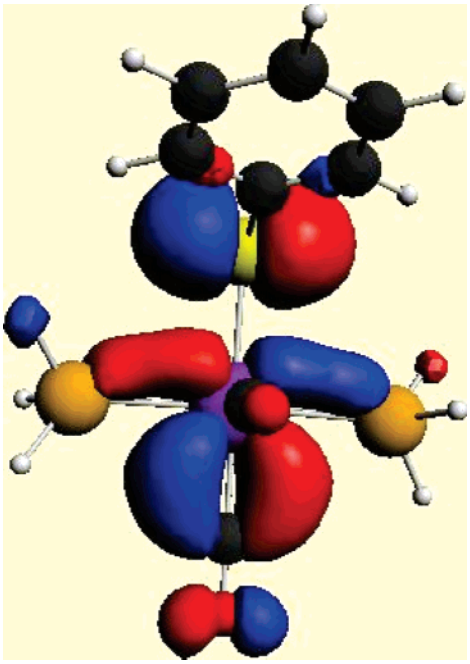

Figure 4. Calculated probability density contour for SOMO of Mo(•SPh)-$(CO)_3(PH_3)_2$.

$(CO_3)(PH_3)_2$ was found to have a SOMO very similar in appearance to its E = S congener. The odd electron in the TePh case resides more on Te than on Mo, with MDC-q spin densities as follows: Te, −0.44; Mo, −0.39. Additionally there is less calculated spin density on atoms other than Te and Mo than there was for the SPh case.

Calculation of the SOMO also yields important insight into the chemical bonding in M(•SPh)$(PR_3)_2(CO)_3$. Because EPh is a π-donor and the t_{2g} orbital set is filled at the metal for these systems, when SPh binds as an *anion* in the complex $M(SPh)(PR_3)_2(CO)_3^-$, there is no net π bond (4e repulsion). In the neutral *radical* a single electron is removed from the Mo−S π^* orbital for a π bond order of one-half. This may have consequences in the net bond strength in the radical. For example it was observed earlier that enhanced stability of the M(•SPh)$(PR_3)_2(CO)_3$ radical may explain the fact that thiophenol bound to $M(PR_3)_2(CO)_3$ undergoes facile H atom transfer[11]

Thermochemistry of Oxidative Addition of PhE−EPh. Solution calorimetric data on the thermochemistry of oxidative addition of dichalcogenides as shown in eq 1 for the full range of S, Se, and Te derivatives of $Mo(P^iPr_3)_2(CO)_3$ and $W(P^iPr_3)_2(CO)_3$ are collected in Table 4. Data for enthalpies of oxidative addition are used to generate bond strength estimates based on recently generated values for PhE−EPh bond strengths.[21] Data for PhS−SPh and $W(P^iPr_3)_2(CO)_3$ were reported earlier, but are repeated here.[11c] Also shown in Table 4 are data reported earlier[22] for $Mo(N[^tBu]Ar)_3$.

Table 4. Enthalpies of Oxidative Addition and Derived M−EPh Bond Strength Estimates

		$Mo(P^iPr_3)_2(CO)_3$[b]		$W(P^iPr_3)_2(CO)_3$[b]		$Mo(N[^tBu]Ar)_3$[c]	
E	E–E[a]	ΔH_{rxn}	BDE	ΔH_{rxn}	BDE	ΔH_{rxn}	BDE
S	46	−30.4	(38)	−42.2[d]	(44)	−63.2	(55)
Se	41	−27.8	(34)	−37.0	(39)	−62.8	(52)
Te	33	−21.4	(27)	−34.0	(33)	−48.0	(41)

[a] All data in kcal/mol. Data for the PhE−EPh bond strength as a function of E are taken from ref 21. [b] Enthalpies of oxidative addition in toluene solution at 25 °C and derived M−EPh bond strengths in kcal/mol. Error limits on calorimetric measurements are typically ±1 kcal/mol. Derived absolute bond strengths in toluene solution are considered accurate to ±3 kcal/mol. [c] Data for PhE−$Mo(N[^tBu]Ar)_3$ used to calculate bond strengths here have been reported previously.[22] [d] Value repeated and slightly revised from earlier data.[11]

The data in Table 4 allow comparison of the bond strengths to $Mo(P^iPr_3)_2(CO)_3$, $W(P^iPr_3)_2(CO)_3$, and $Mo(N[^tBu]Ar)_3$. For the $M(P^iPr_3)_2(CO)_3$ complexes, oxidative addition to W is about 12 kcal/mol more exothermic than for Mo for all three chalcogenides. As a direct result, the W−EPh bond is ∼6 kcal/mol stronger than the Mo−EPh bond in this system. Considering that the bonding radii of Mo and W are typically the same, this indicates the increased coordinating power of W in the complexes $M(PR_3)_2(CO)_3$. Whether or not this difference may be extrapolated to $W(N[^tBu]Ar)_3$ compared to $Mo(N[^tBu]Ar)_3$ is at present unknown.

Oxidative addition to $Mo(N[^tBu]Ar)_3$ is consistently more exothermic than to $Mo(P^iPr_3)_2(CO)_3$. The experimentally observed enthalpies of oxidative addition are nearly twice as exothermic and the Mo−EPh bond is some 14−18 kcal/mol stronger. It should be kept in mind that $M(P^iPr_3)_2(CO)_3$ has a three-center C−H agostic bond blocking its vacant site with a bond strength on the order of 10 kcal/mol and does not possess a truly vacant site.[8] This would reduce both the exothermicity of the oxidative addition reactions and the defined measure of the bond strength in the complexes $M(P^iPr_3)_2(CO)_3$ if no agostic interaction were present. Such an accounting might be of interest for interpreting theoretical results, but for practical utility in terms of reaction mechanisms, and in the formal definition of bond strength, it is the reactions of $M(P^iPr_3)_2(CO)_3$ with its agostic bond present that are observed.

A direct outcome of the data in Table 4 is the ability to calculate the net energy change for direct radical cleavage reactions such as that shown in eq 2:

$$L_nM + PhE{-}EPh \rightarrow L_nM\text{-}EPh + {}^{\bullet}EPh \qquad (2)$$

	calcd ΔH_{rxn}, kcal/mol		
$Mo(CO)_3(P^iPr_3)_2$	E = S (+8)	Se (+7)	Te (+6)
$W(CO)_3(P^iPr_3)_2$	E = S (+2)	Se (+2)	Te (0)
$Mo(N[^tBu]Ar)_3$	E = S (−12)	Se (−11)	Te (−9)

Reaction 2 represents what could be a potential first step in oxidative addition in which a free •EPh radical would be generated. Beneath the equation are shown the calculated enthalpies of this radical cleavage step obtained using data from Table 4. It is clear that for $Mo(N[^tBu]Ar)_3$ this reaction is exothermic for all three dichalcogenides and that for $Mo(P^iPr_3)_2(CO)_3$ it is endothermic. For the complex $W(P^iPr_3)_2(CO)_3$, radical cleavage is calculated to be essentially thermoneutral.

(22) Mendiratta, A.; Cummins, C. C.; Kryatova, O. P.; Rybak-Akimova, E. V.; McDonough, J. E.; Hoff, C. D. *Inorg. Chem.* **2003**, *42*, 8621.

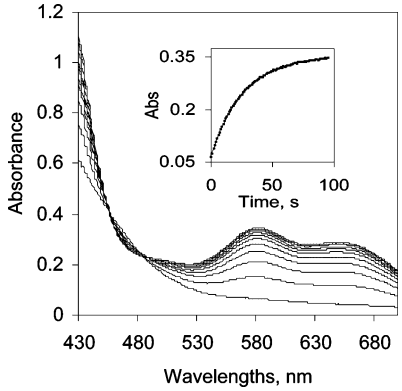

Figure 5. Time-resolved (100 s scan, 10 s intervals) spectral changes and kinetic trace (at 580 nm) obtained upon mixing $Mo(N[^tBu]Ar)_3$ (0.45 mM) with Ph_2Se_2 (4.5 mM) in a stopped-flow cell at −40 °C.

These results have implications for kinetic studies discussed below. If the energetics are favorable, simple radical cleavage as shown in eq 2 can prevail. A second mechanism would involve coordination of PhE−EPh to two metal centers prior to cleaving the chalcogen−chalcogen bond. There is precedent for that type of intermediate in that stable complexes have been prepared as shown in eq 3:

$$2W(CO)_5(THF) + PhTe{-}TePh \rightarrow [PhTe{-}TePh][W(CO)_5]_2 \quad (3)$$

Here the low reductive power of the $W(CO)_5$ group enables stable complexes with an intact Te−Te bond to be prepared and structurally characterized.[23]

Rate and Mechanism of Reaction of $Mo(N[^tBu]Ar)_3$ with Ph_2Se_2. This reaction was studied under both pseudo-first-order (large excess PhSe−SePh) and second-order conditions [$Mo(N[^tBu]Ar)_3$] = $^1/_2$[PhSe−SePh]. The kinetic behavior at all conditions studied was in agreement with first-order dependence on both reactants, and the rate law $d[P]/dt = k_{obs}[Mo(N[^tBu]Ar)_3][PhSe{-}SePh]$ was strictly obeyed from −40 to +25 °C. Representative spectroscopic data and calculated and observed kinetic data under first-order conditions are shown in Figure 5.

Concentration experiments using 1:1 to 1:20 ratios of the reagents were performed to determine initial rates of the reaction. A plot of initial rate versus [Se] is a straight line, with intercept close to zero, as shown in Figure 6, and indicates first-order dependence on [PhSe−SePh].

Varying the concentration of Mo complex (0.45 to 0.225 mM) under pseudo-first-order conditions ([Ph_2Se_2] = 4.5 mM) at 25 °C gave the same $k_{1obs} = 0.48\ s^{-1}$ ($k_2 = 213 \pm 7\ s^{-1}\ M^{-1}$). These data suggest that reaction is first-order in Mo complex as well and follows the rate law $v = k_{obs}[Mo(N[^tBu]Ar)_3][Ph_2Se_2]$. An Eyring plot of the derived second-order rate constants is shown in Figure 7. All of the data are consistent with reaction of $Mo(N[^tBu]Ar)_3$ with PhSe−SePh by a mechanism similar to that shown in the upper portion of Scheme 1. Due to the rapid nature of oxidative addition, resolution of k_{obs} into individual rate constants such as those shown in Scheme 1 was not possible.[4]

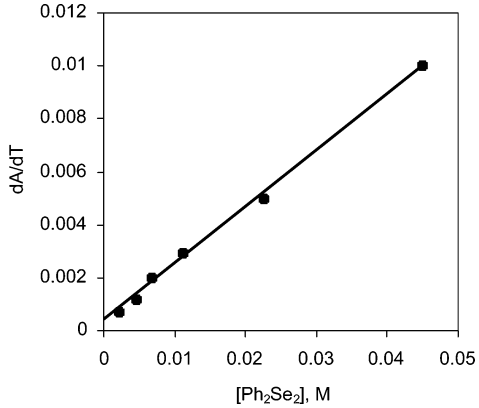

Figure 6. Plot of initial rates of appearance of $[PhSe]Mo(N[^tBu]Ar)_3$ vs [Ph_2Se_2] at −40 °C. The initial concentration of $Mo(N[^tBu]Ar)_3$ was 0.225 mM (before mixing). A least-squares fit of the data gives an intercept of 0.0003 (~3%) ($R^2 = 0.998$).

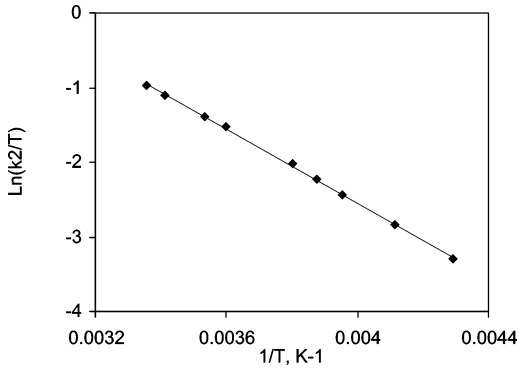

Figure 7. Plot of the temperature dependence of the second-order rate constant for the formation of $(PhSe)Mo(N[^tBu]Ar)_3$ upon mixing $Mo(N[^tBu]Ar)_3$ (0.45 mM) with Ph_2Se_2 (4.5 mM) in toluene. The fit is to the linear form of the Eyring equation, giving activation parameters of $\Delta H^{\ddagger} = 5.0 \pm 0.5$ kcal/mol^{-1}, $\Delta S^{\ddagger} = -32 \pm 4$ eu ($R^2 = 0.999$).

It is of interest to compare the rate of oxidative addition to the rate of ligand binding in this system. The binding of adamantyl isonitrile showed[24] $\Delta H^{\ddagger} = 5.5$ kcal/mol and $\Delta S^{\ddagger} = -15$ cal/mol deg:

$$Mo(N[^tBu]Ar)_3 + AdNC \rightarrow Mo(N[^tBu]Ar)_3(CNAd) \quad (4)$$

The enthalpies of activation for both the ligand binding of AdNC and the oxidative addition of PhSe−SePh are similar within experimental error. It is primarily the entropy of activation that is different for the two processes, and this implies a more ordered transition state for the oxidative addition reaction.

Reaction of $Mo(CO)_3(P^iPr_3)_2$ with Ph_2Se_2. In contrast to the relatively simple picture that emerged for reaction of $Mo(N[^tBu]Ar)_3$ and PhSe−SePh, reaction of $Mo(P^iPr_3)_2(CO)_3$ yielded surprising results. Despite being less thermodynamically favored than $Mo(N[^tBu]Ar)_3$ with respect to oxidative addition (see eq 2), $Mo(P^iPr_3)_2(CO)_3$ was observed to react more rapidly under roughly comparable conditions. All experiments were done in toluene under excess diselenide in the temperature range $T = -80$ to 15 °C, $[Mo(P^iPr_3)_2(CO)_3] = 0.18$ to 0.45 mM, [Ph_2Se_2] = 2.6 mM. Due to the rapid nature of the reaction, it could only be followed using a single wavelength (700 nm). Attempts

(23) Pasynskii, A. A.; Torubaer, Y. V.; Eremenko, I. L.; Vegini, D.; Nefedov, S. E.; Dobrokhotova, A. V.; Yanovskii, A. I.; Struchkov, Y. T. *Russ. J. Inorg. Chem.* **1996**, *41*, 1901.

(24) Stepehens, F. H.; Figueroa, J. S.; Cummins, C. C.; Kryatova, O. P.; Kryatov, S. V.; Rybak-Akimova, E. V.; McDonough, J. E.; Hoff, C. D. *Organometallics* **2004**, *23*, 3126.

to use lower concentrations of the reagents failed due to decomposition of the very air-sensitive $Mo(P^iPr_3)_2(CO)_3$ in highly dilute solution. All measurements were done at $\lambda = 700$ nm, where no photochemistry was expected.

In the temperature interval −80 to −40 °C ([Mo] = 0.45 mM, $[Ph_2Se_2] = 2.6$ mM) attempts to fit the kinetic traces by plotting ln[Mo] versus time yielded curved plots (Figure S3), whereas those for plots of $1/[A_\infty - A]$ (Figure S4) were linear and leave no doubt that at low temperature the reaction is second-order in metal complex. A complete fit to a second-order dependence on $Mo(P^iPr_3)_2(CO)_3$ in the −40 to −80 °C temperature range is shown in Figure S5. At temperatures above −40 °C, deviation from second-order dependence in [$Mo(P^iPr_3)_2(CO)_3$] does not yield such a good fit, indicating a crossover to mixed first-order and second-order dependence on $Mo(P^iPr_3)_2(CO)_3$.

Activation parameters for the −40 to −80 °C temperature range in which second-order dependence on metal concentration is followed are derived from Figure S6 as $\Delta H^\ddagger = 4.4$ kcal/mol and $\Delta S^\ddagger = -28$ cal/mol deg. Surprisingly, under the mM concentration conditions used, the reaction of $Mo(P^iPr_3)_2(CO)_3$, which is second-order in [$Mo(P^iPr_3)_2(CO)_3$], is found to be slightly faster than $Mo(N[^tBu]Ar)_3$, which follows a rate law that is first-order in metal complex. Activation parameters, which overlap within experimental error, are slightly more favorable for reaction of PhSe−SePh with $Mo(P^iPr_3)_2(CO)_3$ compared to $Mo(N[^tBu]Ar)_3$.

In addition to the second-order dependence on metal determined in the rate law, additional support of concerted cleavage is provided by the enthalpy of activation. The fact that it was found to be lower (4.4 kcal/mol) than the estimate for radical cleavage in eq 2 (7 kcal/mol) also supports concerted cleavage. The entropy of activation (ca. −28 cal/mol K) appears to be not as highly negative as might be expected of a ternary transition state [$Mo(P^iPr_3)_2(CO)_3$](PhSe−SePh)[$Mo(P^iPr_3)_2(CO)_3$], which is presumed to be obtained by displacement of the weak agostic bonds by relatively weak dative bonds to selenium. Displacement of the agostic bonds at the metal centers, however, may result in some increased flexibility of the bound isopropyl phosphine ligands and partially compensate for this.

Comparison of Rates of Ligand Binding to $Mo(N[^tBu]Ar)_3$ and $Mo(CO)_3(P^iPr_3)_2$. The more rapid nature of reaction of $Mo(CO)_3(P^iPr_3)_2$ prompted additional qualitative studies. It is clear that the rate of binding of PhSe−SePh plays an integral role in the rate of oxidative addition. Comparison of the rates of ligand binding to the tricyclohexylphosphine derivative $Mo(CO)_3(PCy_3)_2$ versus that to $Mo(N[^tBu]Ar)_3$ can be made based on published literature data. It is known that the complexes $M(CO)_3(PR_3)_2$ (M = Cr, Mo,W) despite having the vacant site blocked by a three-center C−H agostic bond all undergo rapid ligand addition. Kinetic studies performed earlier, however, were reported only for binding of ligands to the cyclohexyl phosphine substituted derivatives and not the isopropyl derivatives studied here. The binding of pyridine shown in eq 5 was determined using previous methodology[8d−g] to have a second-order rate constant of 2.0×10^6 M^{-1} s^{-1} at 298 K:

$$Mo(CO)_3(PCy_3)_2 + py \rightarrow Mo(CO)_3(PCy_3)_2(py) \quad (5)$$

This rate of ligand binding can be compared to the rate of binding[24] of adamantyl isocyanide to $Mo(N[^tBu]Ar)_3$ (pyridine does not bind quantitatively here), for which we extrapolate to 298 K a value of 3.3×10^5 M^{-1} s^{-1}. Thus $Mo(CO)_3(PCy_3)_2$ would be expected to bind ligands roughly 6 times faster at room temperature compared to $Mo(N[^tBu]Ar)_3$. However, rates of ligand addition reported by us earlier were not determined for $Mo(CO)_3(P^iPr_3)_2$. To compare $Mo(P^iPr_3)_2(CO)_3$ to $Mo(PCy_3)_2(CO)_3$, and hence ultimately to $Mo(N[^tBu]Ar)_3$, qualitative competition experiments were performed with regard to binding of AdNC, as shown in eq 6:

$$5Mo(P^iPr_3)_2(CO)_3 + 5Mo(PCy_3)_2(CO)_3 + AdNC \rightarrow \text{Products} \quad (6)$$

Addition of a limited amount of AdNC to excess, equal amounts of both complexes showed that reaction of $Mo(P^iPr_3)_2(CO)_3$ was much faster (roughly estimated as 10−100 times more product) than $Mo(PCy_3)_2(CO)_3$. On the basis of these observations, the rate of ligand binding to $Mo(P^iPr_3)_2(CO)_3$ is estimated to be 2 to 3 orders of magnitude greater than to $Mo(N[^tBu]Ar)_3$.

It was also of interest to compare the rate of ligand binding to that of oxidative addition for $Mo(P^iPr_3)_2(CO)_3$. In a related competition experiment, to a vigorously stirred solution of AdNC and PhSeSePh was slowly added a small amount of $Mo(P^iPr_3)_2(CO)_3$:

$$5AdNC + 2.5PhSe\text{-}SePh + Mo(P^iPr_3)_2(CO)_3 \rightarrow \text{Products} \quad (7)$$

Due to the fact that PhSe−SePh can bind at either of the two Se centers, only 2.5 molar equiv of the oxidant was used. At −70 °C, both $Mo(P^iPr_3)_2(CO)_3(AdNC)$ and $Mo(P^iPr_3)_2(CO)_3(^\bullet SePh)$ were formed in roughly equimolar amounts. This indicates that ligand binding and oxidative addition are competitive reactions[25] even at low T for $Mo(P^iPr_3)_2(CO)_3$.

These observations add support to a mechanism in which rapid ligand exchange occurs for $Mo(P^iPr_3)_2(CO)_3$ resulting in ultimate formation of $Mo(P^iPr_3)_2(CO)_3(PhSe-SePh)Mo(P^iPr_3)_2(CO)_3$, which then undergoes radical cleavage with little barrier. The more rapid nature of reaction of the Mo(0) system studied is attributed to its much greater rate of ligand exchange despite weaker reductive power. Such a mechanism would correspond to the lower pathway in Scheme 1 and would not generate free $^\bullet$SePh radicals. Formation of $Mo(P^iPr_3)_2(CO)_3(PhSe-SePh)$ shown as a reversible equilibrium process in Scheme 1 is logical based on the rapid ligand exchange reactions known to occur for $Mo(PR_3)_2(CO)_3(L)$ complexes[8] and the weak donor ability of neutral organoselenium compounds.

Attempts to Trap $^\bullet$EPh Radicals with $M(CO)_3(PR_3)_2(H_2)$. Chemical evidence for generation of thiyl radicals was generated earlier by us in the case of the oxidative addition of PhS−SPh to $W(CO)_3(PCy_3)_2$. Under an atmosphere of H_2, thiophenol was produced, and the mechanism shown in eqs 8−11 was proposed.[11]

(25) Additional, more quantitative studies of ligand binding for these complexes are planned. The fact that ligand binding of AdNC and oxidative addition of PhSeSePh by $Mo(CO)_3(P^iPr_3)_2$ occur at similar net rates is somewhat surprising. Since oxidative addition presumably incorporates ligand binding as a first step, it is clear that PhSe−SePh must bind equal to or faster than AdNC. The authors could not find data comparing rates of binding at crowded metal centers of Se versus C donor ligands in the literature.

$$W(CO)_3(PCy_3)_2(H_2) \rightarrow W(CO)_3(PCy_3)_2 + H_2 \quad (8)$$

$$W(CO)_3(PCy_3)_2 + PhS\text{-}SPh \rightarrow W(^{\bullet}SPh)(CO)_3(PCy_3)_2 + {}^{\bullet}SPh \quad (9)$$

$$^{\bullet}SPh + W(CO)_3(PCy_3)_2(H_2) \rightarrow W(CO)_3(PCy_3)_2(H^{\bullet}) + HSPh \quad (10)$$

$$W(CO)_3(PCy_3)_2(H^{\bullet}) + PhS\text{-}SPh \rightarrow W(^{\bullet}SPh)(CO)_3(PCy_3)_2 + HSPh \quad (11)$$

In the current work, we have investigated the same reaction qualitatively for $W(CO)_3(P^iPr_3)_2$ and $Mo(CO)_3(P^iPr_3)_2$, where oxidative addition with PhS−SPh and PhSe−SePh was performed under an atmosphere of H_2. At room temperature and a total pressure of 2 atm of H_2, the Mo complex was found to produce no more than trace PhSH (less than 5%) and the W complex gave ∼30% of PhSH, presumably by a mechanism similar to that shown in eqs 8−11. It was thus observed that reactions in keeping with radical cleavage are observed as a greater percentage of the reaction channel for W compared to Mo. This is in keeping with thermochemical data in eq 2, which show a less endothermic nature to direct cleavage to radicals for the W compared to Mo systems.

Additional investigations involved analogous reactions of PhSe−SePh with $Mo(P^iPr_3)_2(CO)_3$ and $W(P^iPr_3)_2(CO)_3$ under H_2. For the Mo system, there was no observation of formation of PhSeH, but the radical $Mo(^{\bullet}SePh)(P^iPr_3)_2(CO)_3$ was formed in high yield. Investigation of oxidative addition of PhSe−SePh with the W complex under H_2 did not produce any free PhSeH. However, the complex $W(^{\bullet}SePh)(P^iPr_3)_2(CO)_3$ was not formed quantitatively, and additional uncharacterized organometallic complexes were formed. This implies that if the PhSe$^{\bullet}$ radical was generated as shown in eq 9, then it did not take part in reactions leading to free PhSeH but may have undergone some additional unknown reaction.

In summary, only for the combination of PhS−SPh and $W(P^iPr_3)_2(CO)_3(H_2)$ was significant PhEH found when oxidation was performed under an atmosphere of H_2. This observation implies that $^{\bullet}$SPh was generated in the reaction and abstracted H from $W(P^iPr_3)_2(CO)_3(H_2)$. The lower (trace or less) yield of PhSH for corresponding reactions of $Mo(P^iPr_3)_2(CO)_3(H_2)$ is in keeping with a lower percentage of oxidative addition proceeding through a free radical mechanism. These observations are also in keeping with the thermochemical data in eq 2.

Reaction of $Mo(^{\bullet}SePh)(P^iPr_3)_2(CO)_3$ and $Mo(N[^tBu]Ar)_3$. Thermochemical data in Table 4 indicate that reaction 12 is exothermic by approximately 10 kcal/mol:

$$Mo(^{\bullet}SePh)(CO)_3(P^iPr_3)_2 + Mo(N[^tBu]Ar)_3 \rightarrow Mo(CO)_3(P^iPr_3)_2 + Mo(N[^tBu]Ar)_3(SePh) \quad (12)$$

Furthermore, the Mo−SePh bond strength in the radical complex (34 kcal/mol) is actually weaker than the PhSe−SePh bond (41 kcal/mol), as discussed above. The fact that oxidative addition of PhSe−SePh to both $Mo(P^iPr_3)_2(CO)_3$ and $Mo(N[^tBu]Ar)_3$ occurs rapidly enough that it must be followed by stopped-flow kinetics prompted qualitative investigation of the $^{\bullet}$SePh group transfer in eq 12. In keeping with thermochemical predictions, FTIR study of reaction 12 showed it to occur over a time period of 1 or 2 h under millimolar concentration conditions at room temperature. The slow nature of this thermodynamically favored group transfer is attributed primarily to steric repulsive forces in the presumed $(P^iPr_3)_2(CO)_3Mo(\mu\text{-}^{\bullet}SePh)Mo(N[^tBu]Ar)_3$ transition state.

Conclusions

Preparation of a full set of $M(^{\bullet}EPh)(P^iPr_3)_2(CO)_3$ complexes is reported as well as investigation of their kinetic, thermodynamic, and spectroscopic properties. These reactions are compared to those for $Mo(N[^tBu]Ar)_3(EPh)$ complexes in terms of bond strength and rate of reaction. Thermochemical factors play an important role in determining whether direct cleavage of the PhE−EPh bond to radicals is uphill for $Mo(P^iPr_3)_2(CO)_3$, approximately thermoneutral for $W(P^iPr_3)_2(CO)_3$, or significantly exothermic for $Mo(N[^tBu]Ar)_3$.

The mechanism of oxidative addition of PhSe−SePh to $Mo(P^iPr_3)_2(CO)_3$ is second-order in metal complex at low temperature, in keeping with a concerted cleavage of PhSe−SePh by coordination of two metals in the transition state. In contrast, first-order (in metal) cleavage of PhSe−SePh is observed for $Mo(N[^tBu]Ar)_3$. This is in keeping with the greater Mo−EPh bond strength observed for $Mo(N[^tBu]Ar)_3$. The most surprising result of this work is that, despite second-order dependence on metal complex, oxidative addition is more rapid for $Mo(P^iPr_3)_2(CO)_3$. This is attributed to a much faster rate of ligand binding to $Mo(P^iPr_3)_2(CO)_3$ compared to $Mo(N[^tBu]Ar)_3$, albeit via what is proposed to be a concerted reaction not involving generation of free $^{\bullet}$EPh radicals. In view of the importance of $^{\bullet}$EPh radicals (either free or trapped at a metal complex), additional studies of these and related reactions by thermodynamic, kinetic, and theoretical methods are in progress.

Acknowledgment. The authors thank the National Science Foundation for funding via grant CRC 0209977. G.J.K. is grateful to the Department of Energy, Office of Basic Energy Sciences, Chemical Sciences Division, for funding. Special thanks to Dr. Joshua Telser, Roosevelt College, for helpful discussions regarding ESR data.

Supporting Information Available: Figure S1 showing FTIR data for $Mo(^{\bullet}EPh)(P^iPr_3)_2(CO)_3$ complexes; Figure S2 showing UV−vis study of formation of $Mo(N[^tBu]Ar)_3(SePh)$; Figure S3 showing first-order kinetic plot for reaction of Ph_2Se_2 and $Mo(P^iPr_3)_2(CO)_3$ at −80 °C; Figure S4 showing second-orderkinetic plot for reaction of Ph_2Se_2 and $Mo(P^iPr_3)_2(CO)_3$ at −80 °C; Figure S5 showing complete best fit data from −40 to −80 °C for $Mo(CO)_3(P^iPr_3)_2 + Ph_2Se_2$ to second-order dependence on metal complex concentration; Figure S6 showing Eyring plot for reaction of $Mo(P^iPr_3)_2(CO)_3$ and Ph_2Se_2; tables of crystal data, 24 pages, including crystal data and structure refinement, atomic coordinates and equivalent isotropic displacement parameters, bond lengths and angles, anisotropic displacement parameters, hydrogen coordinates, isotropic displacement parameters, as well as full data in CIF format. This material is available free of charge via the Internet at http://pubs.acs.org.

JA063250+